AIAA SciTech Forum
8–12 January 2018, Kissimmee, Florida
2018 AIAA Aerospace Sciences Meeting

10.2514/6.2018-1741



# Integrated Assessment of Vehicle-level Performance of Novel Aircraft Concepts and Subsystem Architectures in Early Design

Yu Cai*, Imon Chakraborty†, and Dimitri N. Mavris‡
*Aerospace Systems Design Laboratory, School of Aerospace Engineering,*
*Georgia Institute of Technology, Atlanta, Georgia, 30332*



**Future technology-integrated commercial transports are expected to have significant fuel saving and performance improvements which are likely beyond the capability of today's conventional aircraft designs. Advanced concepts such as the hybrid wing-body configuration are predicted to have potential fuel benefits over the conventional tube-and-wing configuration. Meanwhile, aircraft subsystems are also evolving towards More Electric architectures which may achieve fuel saving through more efficient secondary power usage. While vehicle performance over the design mission is an important consideration in the design process, off-design mission performance also influences real-world airline operations. In this work, the Integrated Subsystems Sizing and Architecture Assessment Capability (ISSAAC), an existing integrated environment for tube-and-wing aircraft and subsystem sizing and analysis, is enhanced to perform hybrid wing-body aircraft subsystem sizing and analysis as well as off-design mission performance analysis. A combinatorial set of subsystem architectures are evaluated to investigate the impact of different subsystem architectures on vehicle-level weight and performance. Sensitivity analyses are also performed for a down-selected set of architectures to assess the impact of uncertainties on the vehicle-level performance.**

## I. Introduction

In 2010, the National Aeronautics and Space Administration's (NASA) Environmentally Responsible Aviation (ERA) project[1] established a set of performance and environmental goals for future technology-integrated commercial transports for the 2020 time frame (N+2), as presented in Table 1. The goals include simultaneous reduction in noise, emissions, fuel burn, and required field length. Performance improvements of this magnitude are likely beyond the capability of conventional tube-and-wing (TW) configurations. Therefore, novel aircraft concepts are highly desired, for example, the hybrid wing-body (HWB) configuration.

**Table 1. Target N+2 time frame performance improvements relative to a large twin-aisle reference configuration[1]**

| Metric | Technology Benefits by 2020 (N+2) |
|---|---|
| Noise (cumulative below Stage 4) | −42 dB |
| LTO NOx Emissions (below CAEP 6) | −75% |
| Performance: Aircraft Fuel Burn | −50% |
| Performance: Field Length | −50% |

In literature, it has been claimed that HWB designs have potential benefits over TW designs on certain design missions,[2–7] while some known challenges have also been discussed, such as actuation power for

*Graduate Research Associate, ASDL, School of Aerospace Engineering, Georgia Tech, AIAA Student Member
†Research Engineer II, ASDL, School of Aerospace Engineering, Georgia Tech, AIAA Member
‡S.P. Langley Distinguished Regents Professor and Director of ASDL, Georgia Tech, AIAA Fellow

controls[6,7] and structural weight estimation.[8,9] In addition, improvements are also required for aircraft subsystem architecture. Driven by the More Electric Aircraft Initiative,[10] some recent aircraft have introduced novel subsystem architectures, with one representative example being the Boeing 787 aircraft which features a "no-bleed" architecture.[11] With unconventional configurations, such as the HWB, and more efficient use of secondary (non-propulsive) power, aircraft may achieve a better fuel efficiency than conventional TW designs. On the other hand, the sizing and trade-off analyses for novel system architectures, which affect the sizing and performance of the aircraft, have not been thoroughly investigated for the HWB.

Previous research has focused on various aspects of the HWB design, including configuration and sizing,[2] design mission performance analysis,[4,5] aerodynamics,[2] structure,[2,8,9] propulsion system,[4] control surface layout and actuation,[2,6,7] emission and noise,[12] etc. The following list provides a review of some highlighted results on sizing and mission performance analysis of HWB configuration.

- In an HWB configuration scaling study,[5] Nickol concluded that the potential fuel burn benefit of HWB over conventional tube-and-wing (TW) increases as the product of design payload and design range increases, with a predicted fuel saving of approximately 5.5% for a 300-pax class HWB. However, the sensitivity of predicted HWB fuel benefit to vehicle empty weight and overall drag coefficient is also significant: a 10% increase in predicted empty weight or a 10% increase in predicted drag could wash out all potential fuel benefits of HWB.

- Felder et al.[4] examined a concept of turbo-electric distributed propulsion system on a 300-pax HWB aircraft. A 70-72% reduction in design mission fuel burn was estimated compared to a conventional TW baseline of the same seating class, a Boeing 777-200LR-like vehicle. However, this result was based on assumption of component weights (such as for the transmission cables) and expected future technology state-of-the-art (SOTA), whereas uncertainty in these parameters may have significant impact on the estimated fuel benefit.

- Liebeck[2] predicted that an 800-pax long-haul HWB can achieve 27% fuel benefit on the design mission compared to a similar-sized conventional TW vehicle. It was also pointed out that HWB designs are faced with issues and risks which applied for TW configuration back in early Jet Age (1950s). These include complex flight control architecture and allocation, large auxiliary power requirements, long-range performance, and limited historical data for commercial transports.

Through literature review, it can be observed that the predicted fuel benefit of HWB over TW varies significantly between studies, due to differences in design requirements, system architectures, as well as study ground rules and technology assuptions. Therefore, an integrated environment for automatic evaluation of large architecture space and assessment of such uncertainty parameters is needed. This study attempts to perform integrated subsystems sizing and aircraft performance analysis for HWB configurations, aiming ultimately to generate insight regarding the best-performing architectures, and to identify the uncertainty factors they are most sensitive to. The basis of HWB subsystem sizing and analyses is an existing framework, the *Integrated Subsystem Sizing and Architecture Assessment Capability* (ISSAAC), which is suitably modified and enhanced to permit assessment of HWB configurations.

The remainder of this paper is organized as follows: Section II provides a summary overview of the enhanced ISSAAC environment. Section III describes the subsystem architectures considered on the HWB as well as the baseline 300-pax class vehicle (HWB300) with a conventional subsystem architecture. Section IV and V describe the power consuming subsystems and power generation and distribution subsystems considered in this work. Section VI introduces the capability of off-design mission performance analysis which applies for both conventional TW vehicles and unconventional (e.g., HWB) vehicles. Section VII compares the performance of different architectures. Finally, Section VIII concludes the paper and highlights avenues for future work.

## II. Integrated Subsystem Sizing and Architecture Assessment Capability

The tool used to size HWB vehicle and its subsystem architectures is an enhancement of the *Integrated Subsystem Sizing and Architecture Assessment Capability* (ISSAAC), which consists of different modules linking the sizing and analysis of aircraft subsystems for TW configuration. A detailed description of the first version of ISSAAC (V1) can be found in separate works.[13–15] As part of this research, ISSAAC is upgraded to a second version (V2) which incorporates the capability of analyzing the subsystem architectures on HWB

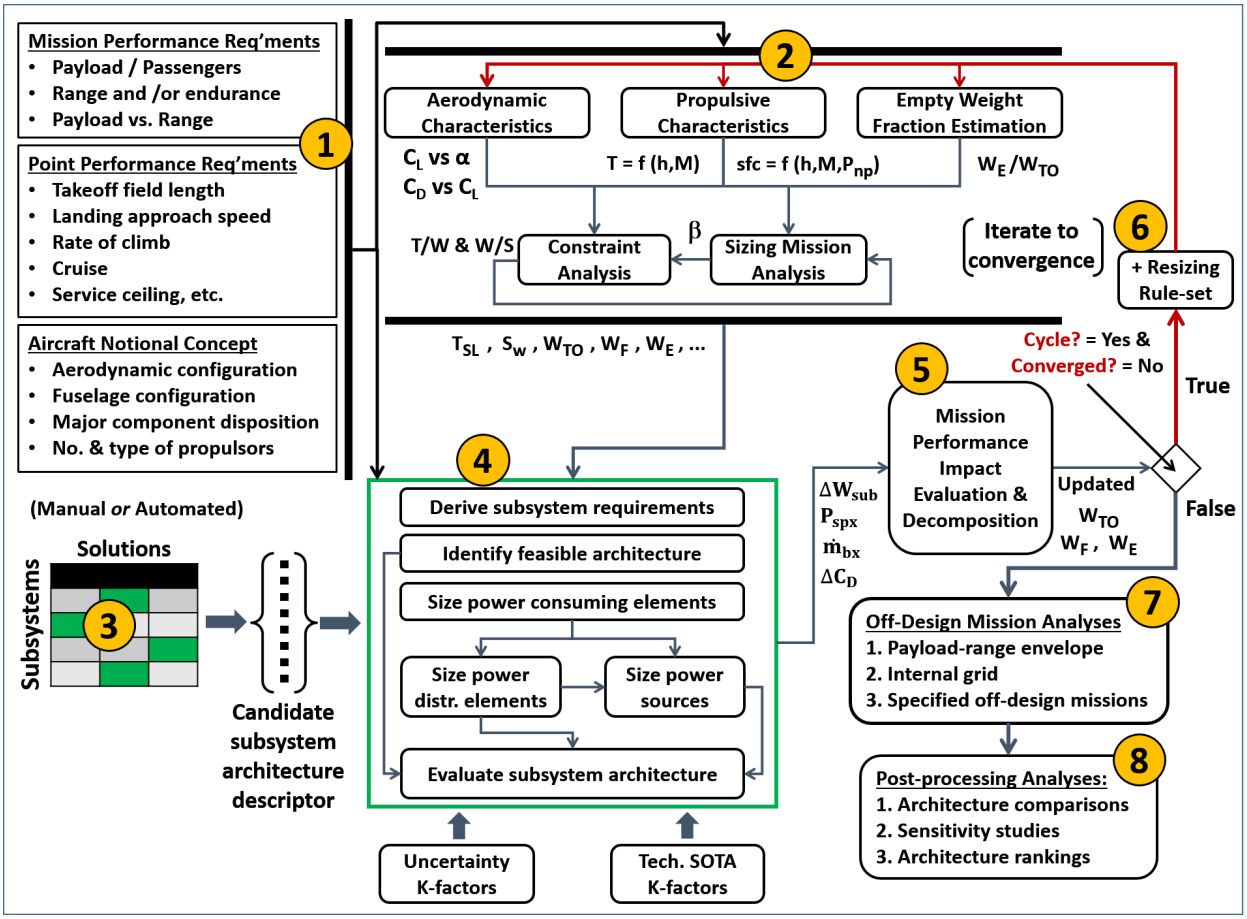


**Figure 1. Main modules of Integrated Subsystem Sizing and Architecture Assessment Capability (ISSAAC)**

vehicles, as well as the capability of evaluating off-design mission performance of a sized vehicle. The main modules of ISSAAC V2 are depicted in Fig. 1 and briefly described below.

1. **Definition of design requirements.** The design requirements include the mission performance requirements (e.g., payload capacity, design payload, and design range), the point performance requirements (e.g., cruise speed, rate of climb, and service ceiling), and the aircraft notional concept (e.g., TW or HWB configuration and engine characteristics).

2. **Traditional aircraft & engine sizing.** This module defines the aircraft in terms of a geometric scale (such as the reference wing planform area $S_w$), a propulsive scale (such as the required sea-level static thrust $T_{SL}$), and key weights (such as the takeoff gross weight $W_{TO}$ and the empty weight $W_e$). The vehicle sizing and mission analysis is done using Flight Optimization System (FLOPS) developed by NASA Langley Research Center,[3,16] while the corresponding parametric engine deck is generated using Numerical Propulsion System Simulation.[17] The subsystem weight buildup relationships within FLOPS (and most other similar tools) are based on regressions of historical data, and therefore apply to conventional subsystem architectures.

3. **Candidate subsystem architecture descriptor.** This module provides a qualitative description of the subsystem architecture to be evaluated. For example, an architecture descriptor may indicate whether a subsystem consumes hydraulic, electric, or pneumatic power. For automatic evaluation of a large architecture space, the descriptors may be predefined in the form of a Matrix of Alternatives (MoA), as shown in Fig. 1.

4. **Subsystem architecture sizing and evaluation.** This module performs sizing of the major power consuming elements, power distribution elements, and power sources within the subsystem architecture

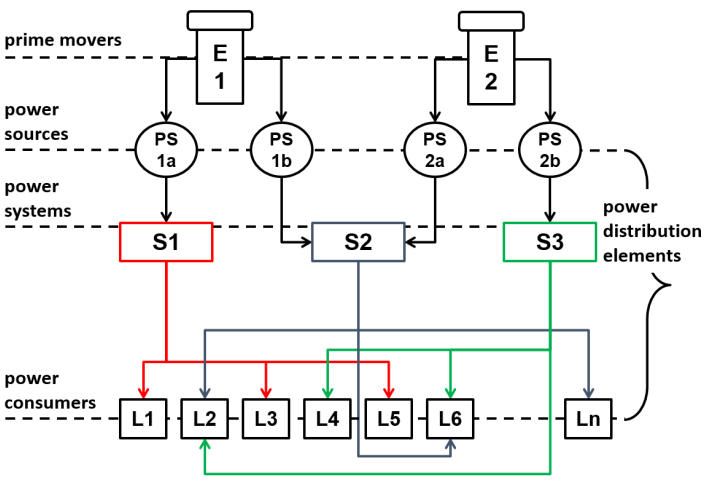


(a) Generalized representation of elements and connectivity within an aircraft subsystem architecture

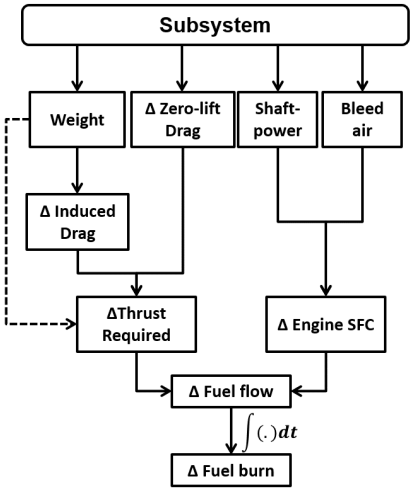


(b) Impact of subsystems on fuel consumption (mission-level metric)

**Figure 2.**

(a generalized representation of which is shown in Fig. 2(a)). The outputs are the mass breakdown, the overall change in subsystem weight $\Delta W_{sub}$, and the time histories of shaft-power requirement $P_{spx}(t)$, bleed air requirement $\dot{m}_{bx}(t)$, and direct drag increment $\Delta C_{D_0}(t)$ of the considered architecture. The latter three mission-specific and potentially time-varying quantities are computed for the design mission and off-design missions (if any), for each subsystem and also for the architecture as a whole. The environment automatically detects the vehicle configuration (TW or HWB) as defined in Module 1 and applies the appropriate sizing method for each subsystem (Sec. IV and V).

5. **Design mission performance analysis.** This module evaluates the impact of the considered subsystem architecture on the design mission performance. As shown in Fig. 2(b), the impact occurs through weight, secondary power requirements, and drag increments, which are computed in Module 4. The fuel impact of change in vehicle empty weight $\Delta W_{sub}$ is first captured by propagating this term in a FLOPS call. Then, the following equation system is then solved backward in time (from landing, $k = n$, to takeoff, $k = 1$), to compute the fuel impact of the secondary power extraction and drag increment. The goal is to solve for the change in fuel required at takeoff $\Delta W_f^{(TO)} = \Delta W_f^{(1)}$.

$$\Delta C_L^{(k)} = \frac{\Delta W_f^{(k+1)}}{q^{(k)} S_w} \tag{1a}$$

$$\Delta C_{D_i}^{(k)} = C_{D_i}(C_{L,0}^{(k)} + \Delta C_L^{(k)}) - C_{D_i}(C_{L,0}^{(k)}) \tag{1b}$$

$$\Delta D_{ddl}^{(k)} = q^{(k)} S_w \, \Delta C_{D_i}^{(k)} \tag{1c}$$

$$\Delta D_{dil}^{(k)} = q^{(k)} S_w \, \Delta C_{D_0}^{(k)} \tag{1d}$$

$$\Delta D^{(k)} = \Delta D_{ddl}^{(k)} + \Delta D_{dil}^{(k)} \tag{1e}$$

$$\Delta T^{(k)} = \Delta D^{(k)} + \Delta W^{(k+1)} \left( \frac{\dot{h}}{V} + \frac{1}{g} \dot{V} \right)^{(k)} \tag{1f}$$

$$T^{(k)} = T_0^{(k)} + \Delta T^{(k)} \tag{1g}$$

$$\Delta \dot{w}_f^{(k)} = \dot{w}_f \left( h^{(k)}, M^{(k)}, T^{(k)}, P_{spx}^{(k)}, \dot{m}_{bx}^{(k)} \right) - \dot{w}_f \left( h^{(k)}, M^{(k)}, T_0^{(k)}, 0, 0 \right) \tag{1h}$$

$$\Delta W_f^{(k)} = \Delta W_f^{(k+1)} + \Delta \dot{w}_f^{(k)} \, \Delta t^{(k)} \tag{1i}$$

$$k = k - 1, \text{ and repeat sequence}$$

$$\text{Start point: } k = n - 1, \qquad \Delta W_f^n = 0 \tag{1j}$$

In the above equation system, $C_L$ is the lift coefficient; $C_L$ is the lift coefficient; $C_{D_i}$ is the induced drag coefficient, as a function of the $C_L$; $C_{D_0}$ is the zero-lift drag coefficient; $D_{ddl}$ is the drag dependent on lift; $D_{dil}$ drag independent of lift; $T$ is the thrust; $\dot{w}_f$ is the fuel flow; $W$ is the vehicle gross weight; $W_f$ is the fuel weight; $h$ is the altitude; $V$ is the velocity; $M$ is the Mach number, and $q$ is the dynamic pressure. The symbol $\Delta$ denotes the increment of a parameter $(\cdot)$ relative to its reference value $(\cdot)_0$ for the same mission where the weight, secondary power extraction, and drag increments are not considered.

6. **Resizing of aircraft & subsystems.** Due to the impact of subsystem architecture, the vehicle may either fly a longer range carrying the design payload, or fail to operate the design mission. This optional module iteratively resizes the aircraft and its subsystems based on certain resizing rules, until the design performance satisfies the requirements specified in Module 1. In this study, the vehicle is retrofitted instead of being resized, which means that the essential geometry of the aircraft (e.g., fuselage, wing, and tail geometry) remains unchanged unless directly influenced by the subsystem architecture.

7. **Off-design mission performance analysis.** The off-design mission performance may be optionally evaluated after analysis of design mission performance and resizing (if chosen). The off-design mission performance evaluation includes the determination of the payload-range envelope and the mission-specific fuel consumption and vehicle takeoff weight within the envelope (Sec. VI).

8. **Post-processing analyses.** This module can be customized depending on the type of analysis being performed. In this work, an combinatorial space of subsystem architectures are first evaluated to investigate their impact on vehicle weight and mission performance. Then, a few representative subsystem architectures are selected to perform sensitivity analyses on modeling and technological uncertainty factors. MATLAB and JMP are involved in these post-processing analyses.

## III. Subsystem Architecture Space and Baseline Aircraft

The architecture space includes both conventional and More Electric architectures. In each architecture, subsystems are categorized by the type of secondary power consumed and their own attributes, such as the type of actuators or operation mode, etc. For example, the environmental control system (ECS) may be simply classified as pneumatic or electric, based on the type of secondary power it uses to pressurize the cabin.[13] The case for flight control actuation system and ice protection system are more complex, as discussed below.

**Table 2. Electrified flight control actuation packages considered**

| Actuation Function | Actuation Package | | | | | | |
|---|---|---|---|---|---|---|---|
| | P-0 | P-1 | P-2 | P-3 | P-4 | P-5 | P-6 |
| TRAS | – | ✓ | ✓ | ✓ | ✓ | ✓ | ✓ |
| WBS | – | ✓ | ✓ | ✓ | ✓ | ✓ | ✓ |
| LGAS | – | – | ✓ | ✓ | ✓ | ✓ | ✓ |
| NWSS | – | – | ✓ | ✓ | ✓ | ✓ | ✓ |
| FCAS-Slat | – | – | – | ✓ | ✓ | ✓ | ✓ |
| FCAS-Prim. | – | – | – | – | H/EHA | EHA | EMA |

✓ – Electrified actuation function
EHA – Electrohydrostatic actuator
EMA – Electromechanical actuator
H/EHA – Hydraulic actuator & EHA in parallel
Prim. – Primary flight control surfaces

In a certain architecture, the actuation functions, including the flight control surface actuation system (FCAS), landing gear actuation system (LGAS), wheel brake system (WBS), nose wheel steering system (NWSS), and thrust reverser actuation system (TRAS), may consume hydraulic or electric power, and use

different types of actuators. Table 2 presents the seven actuation packages considered in this work, where more actuation functions become electrified as the package number increases. The reader is referred to previous work[13] for a detailed discussion on the characteristics of each actuation package as well as the rationale behind such progressive electrification of the actuation functions.

The wing ice protection system (WIPS) and the cowl ice protection system (CIPS) may consume either pneumatic power (P) or electric power (E). Depending on the amount of heat supplied, both systems can be classified as evaporative (Ev) or running-wet (RW). Furthermore, based on the system operation mode, they may also be classified as anti-icing (AI) or de-icing (DI). These three attributes, if assumed independent, result in a total of eight ($2^3$) alternatives for each ice protection system. However, due to operational constraints, not all of the eight alternatives may be implemented on both ice protection systems.[13] In this work, four options are considered for each ice protection system, as shown in Table 3.

**Table 3. Combinatorial space of subsystem architectures considered**

| Subsystem | Options | Number |
|---|---|---|
| Actuation functions (AFP) | P-0, P-1, P-2, P-3, P-4, P-5, P-6 | 7 |
| Wing ice protection (WIPS) | P-Ev-AI, P-RW-AI, E-RW-AI, E-RW-DI | 4 |
| Cowl ice protection (CIPS) | P-Ev-AI, P-RW-AI, E-Ev-AI, E-RW-AI | 4 |
| Environmental control (ECS) | Pneumatic, Electric | 2 |
| | **Total number of combinations:** | 224 |

Based on the above discussion, the options of actuation function packages (AFP), WIPS, CIPS, and ECS form a combinatorial architecture space of 224 candidates, as shown in Table 3. For convenience, each candidate may be described using a numerical descriptor as defined in Fig. 3, where the example describes a candidate equipped with AFP-#4, an electrothermal running-wet anti-icing WIPS, a pneumatic evaporative anti-icing CIPS, and an electric ECS.

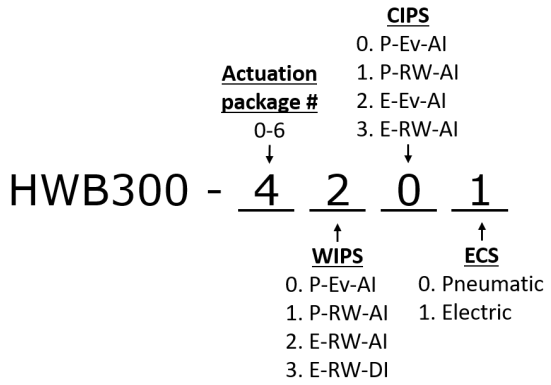


**Figure 3. Candidate subsystem architecture descriptor**

The vehicle-level impact of subsystem architectures is assessed with reference to a notional 300-pax class HWB aircraft baseline (HWB300) with a conventional subsystem architecture, whose payload-range characteristics are presented in Fig. 4. The baseline characteristics were obtained by evaluating ISSAAC with the vehicle's subsystem architecture set to conventional, i.e., pneumatic ECS and IPS, and hydraulic actuation functions. Some key weights, performance parameters, and geometric parameters are listed in Tables 4 and 5. Since the baseline vehicle model uses an externally calculated drag polar which cannot be scaled with the vehicle geometry within FLOPS thus preventing resizing analysis at this point in time. A retrofit analysis is therefore performed in this study where the vehicle geometry and the engine characteristics remain invariant.

While this baseline model defines the essential vehicle geometry such as the wing, vertical tail, and fuselage dimensions, it does not specify control surface layout, landing gear configuration, ice protected area, and internal arrangement of system components such as generators, actuators, hydraulic and pneumatic

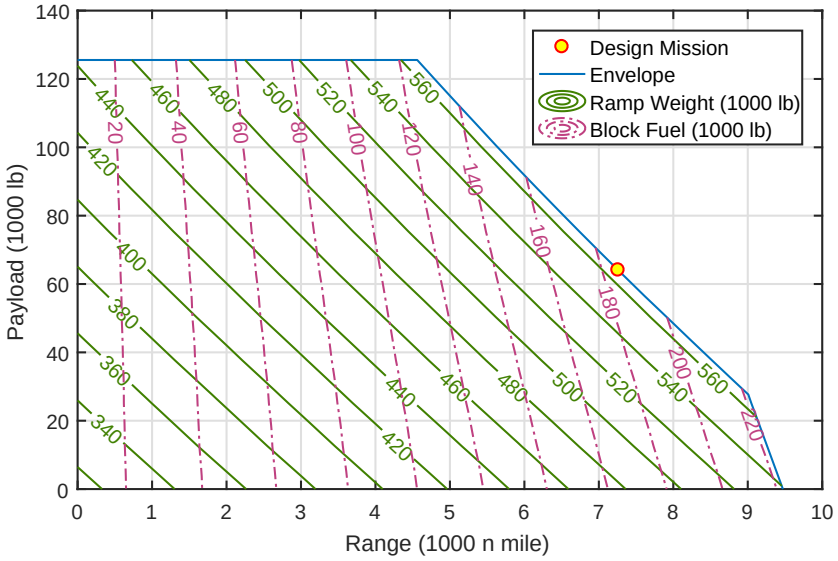


**Figure 4. Payload-range of HWB300 baseline with ramp weight and block fuel contours**

**Table 4. Weight and performance parameters of the HWB300 baseline**

| Parameter | Value | Unit |
|---|---|---|
| Passenger capacity | 305 | - |
| Design payload weight | 64,050 | lbm |
| Design range | 7260 | n mile |
| Harmonic range | 4560 | n mile |
| Ferry range | 9470 | n mile |
| Cruise Mach number | 0.84 | - |
| Maximum cruise altitude | 43,000 | ft |
| Maximum ramp weight | 566,260 | lbm |
| Maximum payload weight | 125,550 | lbm |
| Operating empty weight | 294,200 | lbm |
| Maximum fuel capacity | 244,410 | lbm |
| Sea-level static thrust | 4×33,980 | lbf |

ducts, and electric cables, etc. Due to lack of historical data and existing research on HWB subsystem architectures, assumptions on detailed subsystem configuration will be made in the following discussion in order to estimate the impact of subsystem architectures.

## IV. Modeling of Secondary Power Consuming Subsystems

This work considers the four major secondary power consuming subsystems (PCS) listed in Table 3. The goal of modeling each PCS is to determine its weight breakdown and the variation of its bleed air requirement, shaft-power requirement, and direct drag increment, if any, over the course of all missions considered in the analysis. With this information, the impact on fuel burn of any subsystem architecture can be analyzed following the four paths shown in Fig. 2(b).

Table 5. Geometric parameters of the HWB300

| Parameter | Value | Unit |
|---|---|---|
| Fuselage total length | 120.9 | ft |
| Fuselage maximum height | 20.0 | ft |
| Cabin maximum width | 45.7 | ft |
| Passenger compartment length | 84.6 | ft |
| Wing reference area | 10,655 | $ft^2$ |
| Wingspan | 255.3 | ft |
| Wing reference aspect ratio | 6.12 | - |
| Wing reference taper ratio | 0.311 | - |
| Wing reference thickness-to-chord ratio | 0.11 | - |
| Wing 1/4-chord sweep | 36.0 | deg |
| Wing dihedral | 3.0 | deg |
| Number of vertical tails | 2 | - |
| Vertical tail planform area, each | 140 | $ft^2$ |
| Vertical tail 1/4-chord sweep | 39.4 | deg |
| Vertical tail aspect ratio | 1.95 | - |
| Vertical tail taper ratio | 0.464 | - |
| Vertical tail thickness-to-chord ratio | 0.08 | - |



### A. Actuation Functions

The flight control actuation system (FCAS) includes the surface controls for all control surfaces of the aircraft. A conventional TW transport may have control surfaces such as ailerons, elevators, rudders, spoilers, and high-lift devices (flaps and slats). In most HWB designs, due to the absence of a horizontal tail, which is normally used to trim a TW vehicle, the trailing edge control surfaces cannot be used as flaps.[2] Instead, a redundant number of multi-objective elevons are used on the trailing edge to provide both pitching and rolling moments.[6] In this work, the HWB vehicle is assumed to be equipped with five equal-span elevons and five equal-span leading-edge slats on each side of the outboard wings, plus one rudder on each of the two vertical tails, and two centerbody elevons between the vertical tails, as shown in Fig. 5.

For TW vehicle with conventional ailerons, elevators, rudders, and spoilers, ISSAAC is capable of estimating the maximum hinge moments, holding load, and actuation power consumption of the control surfaces based on the flight envelope, actual flight condition, control surface geometry, and regulation requirements.[13] It has also been noted that the Federal Aviation Regulations (FAR) requirements[18] for TW vehicles appear ambiguous for HWB configuration, e.g., it is not clear how the size of elevons on HWB should comply with the requirements for ailerons on TW vehicles.[6] Therefore, the FCAS sizing method for TW vehicles is not directly applicable to the HWB. In this work, the elevon hinge moments are estimated based on the "baseline" elevon layout in Garmendia et al.'s work,[6] where a Vorlax model for a similar sized HWB vehicle was constructed and validated against wind-tunnel data. The sizing hinge moement of each elevon is summarized in Table 6. The sizing method for rudders is assumed common between TW and HWB vehicles.

The landing gear system of HWB designs is assumed to be similar to that of TW vehicles. The layout of the landing gear, including the number of main landing gear struts and tires, is determined based on maximum vehicle gross weight. Specifically, the HWB300 baseline is assumed to have one nose landing gear leg with two tires and two main landing gear legs, each with six tires. The actuators in the landing gear system may consume either hydraulic or electric power. The actuator mass and power requirement for retraction, extension, nose-wheel steering, and wheel-braking for HWB are estimated in the same way as done for TW vehicles in ISSAAC V1: the brake actuation force and power requirements are based on constraining static and dynamic braking cases; the nose-wheel steering force and power requirements are based on a load condition specified in the Code of Federal Regulations (CFRs); the gear extension and

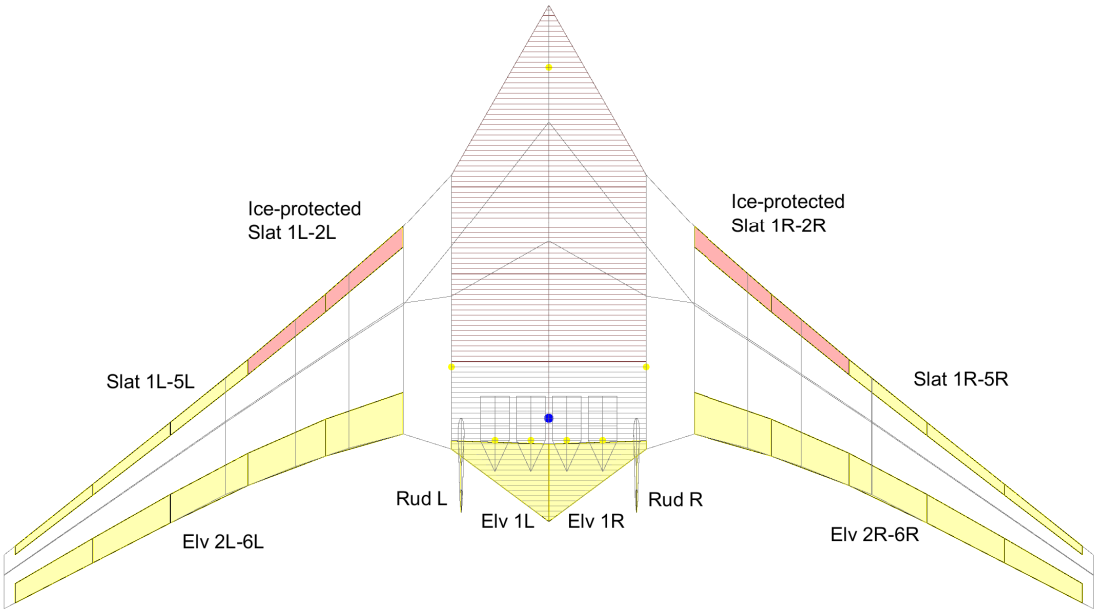


**Figure 5. HWB300 control surface layout and extent of wing ice protection**

**Table 6. Estimated hinge moment of elevons[6] in Fig. 5**

| Elevon ID | Hinge Moment (kN·m) |
|---|---|
| Elv 1L/1R | 65.9 |
| Elv 2L/2R | 30.9 |
| Elv 3L/3R | 33.4 |
| Elv 4L/4R | 22.9 |
| Elv 5L/5R | 16.8 |
| Elv 6L/6R | 31.0 |

actuation power requirements are computed based on a simplified kinematic model and the mass properties of the gear legs.[13] Each engine on the HWB vehicle is assumed to have one thrust reverser, consuming either hydraulic power or electric power. For both types of actuation, the actuator power requirement is estimated using a regression function of the sea-level static thrust, and the actuator mass is estimated based on the sizing power and corresponding actuator power-to-mass ratio, in the same manner as done for TW vehicles in ISSAAC V1.[13]

The mass of an actuator can be determined using a generic formula as shown in Eq. (2):

$$m_{\text{act}} = \frac{\mathcal{X}_0}{(\mathcal{X}_0/m)} \tag{2}$$

where $\mathcal{X}_0$ can be the load or power which the actuator is sized to provide, e.g., the stall load of a linear actuator or the maximum output shaft-power of a power drive unit; $(\mathcal{X}_0/m)$ is the corresponding figure of merit with the current technological state-of-the-art (SOTA), e.g., the force-to-mass ratio or the power-to-mass ratio. Electric actuators contain their own electric motors and power electronics whose mass may also be computed using Eq. (2). An improvement in SOTA of an actuator or its component may be modeled with a multiplicative factor on its figure of merit. For electric actuators, Eq. (3) may be used to compute the actuator mass accounting for improvements in SOTA:[13]

$$m_{\text{act}} = \frac{\mathcal{X}_0}{(\mathcal{X}_0/m)} + \frac{P_m^{\max}}{\eta_m}\left[\frac{1}{(P/M)_{\text{em}}}\left(\frac{1}{\kappa_{\text{em}}} - 1\right) + \frac{1}{\eta_{\text{em}}\eta_{\text{pe}}(P/M)_{\text{pe}}}\left(\frac{1}{\kappa_{\text{pe}}} - 1\right)\right] \tag{3}$$

where $P_m^{\max}$ is the maximum power output of the actuator; $\eta_m$ is the overall component efficiency downstream of the electric motor; $(P/M)_{\text{em}}$ and $(P/M)_{\text{pe}}$ are the power-to-mass ratios of the electric motor and the power electronics, whose improvements are modeled with $\kappa_{\text{em}} > 1$ and $\kappa_{\text{pe}} > 1$; $\eta_{\text{em}}$ and $\eta_{\text{pe}}$ represent their overall efficiencies.

### B. Ice Protection System

The ice protection system considered in ISSAAC includes the wing ice protection system (WIPS) and the cowl ice protection system (CIPS). The major tasks in sizing of WIPS involves determination of the protected surface area, or the leading-edge slats which need protection. However, even on TW configuration, there is no general rule that could be used to perform this task.[13] Since no open literature has done a detailed analysis of IPS on HWB configuration, the method applied in ISSAAC V1 is used to obtain a first estimation of mass and required power for both WIPS and CIPS, where the spanwise extent of the WIPS protected area is governed by the mean aerodynamic chord (the ice-protected slat panels of the HWB300 are highlighted in Fig. 5), and the CIPS protected area is determined based on nacelle diameter and length . The IPS heat flux requirement (rate of heat supply per unit protected area) is determined as a function of flight and atmospheric conditions by evaluating the heat fluxes due to convection, evaporation, sensible heating, and kinetic heating. The product of heat flux and protected area gives the IPS heating requirements.[13]

### C. Environmental Control System

As the single biggest consumer of secondary power in commercial aircraft, ECS provides pressurization, thermal regulation, and ventilation for the aircraft cabin. Most conventional TW transports in history are equipped with pneumatic ECS, while recently some More Electric designs move to electric ECS. In this study, both types of ECS are considered for HWB vehicles. Due to lack of information from open literature, the sizing of ECS on HWB configuration follows the same method as done for TW in ISSAAC V1, where the ECS power required is based on steady-state heat balance equation, taking into account heat loss through the cabin wall, metabolic heat load from occupants, and heat generated due to galley load, lighting, and in-flight entertainment systems.[13]

Previously in ISSAAC V1, a ECS pack thermal model coded as MATLAB functions was used to compute the sizing power and the time-varying secondary power consumption history of both pneumatic and electric ECS packs were directly computed using NPSS, which was a time-consuming process. To enable fast evaluation of the ECS packs while maintaining high fidelity, an innovative approach is introduced in this work, where a physics-based ECS pack NPSS model is queried off-line on a full-factorial grid of operating parameters which include the expected altitude, airspeed, and required cabin air flow properties during typical missions for commercial aircraft. With the sample data, interpolating meta-models of the ECS packs are generated which are then used in ISSAAC V2 to accelerate the computation process. The reader is referred to a separate paper by the authors for the development of the meta-model.[19] In ISSAAC, the pack meta-models are queried in form shown in Eq. (4):

$$T_e = f(\dot{m}_s, P_s, T_s, \dot{m}_r, P_r, T_r) \tag{4}$$

where $\dot{m}_s$, $P_s$, and $T_s$ are the per-pack mass flow, total pressure, and total temperature of the pack supply air, and $\dot{m}_r$, $P_r$, and $T_r$ are the same properties of the colling ram air.

## V. Modeling of Secondary Power Generation and Distribution Subsystems

The secondary power generation and distribution systems (PGDS) are responsible for generating hydraulic, electric, pneumatic, and mechanical power and distributing it to corresponding PCS. For each PGDS, the connectivity between the power generator and consumer is first established taking into account redundancy requirements. Then the power dissipation and mass breakdown of each PGDS are computed based on the system connectivity and consumer power requirements. In this work, it is assumed that the sizing methods of pneumatic/hydraulic ducts, electric cables, pumps, generators, and gearboxes, etc., are common between HWB and TW vehicles. Therefore, this section mainly focuses on the component-to-component connectivity for the HWB configuration, while the reader is referred to Chakraborty's work[13] for details on the sizing process.

As the first step of sizing PGDS, a topological diagram showing its logical connectivity is established based on the subsystem architecture, which specifies the consumers of each type of secondary power. Next, the topological diagram is translated into physical connectivity by mapping each element to its spatial location in the vehicle, as shown in Fig. 6. In the topological diagram, every element is parametrically located using dimensionless geometric coordinates relative to its parent (fuselage, wing, tail, nacelle, etc.). For example, if the wing is resized, then the control surfaces, actuators, WIPS area, hydraulic ducts, and electric cables are automatically resized. The hydraulic pumps and electric generators are also resized accordingly based on the updated secondary power requirement.

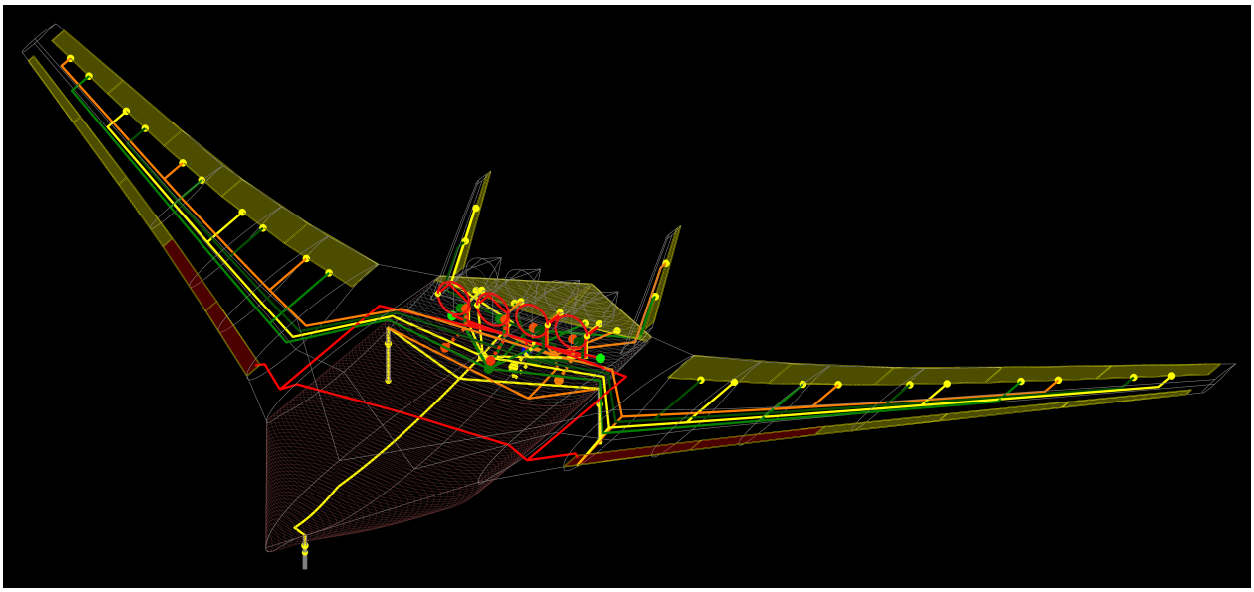

**Figure 6. Physical connectivity in aircraft geometric model of HWB300-4000**

### A. Pneumatic Power Generation and Distribution System

The pneumatic power generation and distribution system (PPGDS) is present if ECS, WIPS, and/or CIPS is pneumatic. Figure 7 is the topological diagram of PPGDS for architectures where the ECS, WIPS, and CIPS consume pneumatic power. Note that it pertains to the four-engine configuration of HWB300, but can be generalized to other configurations. The CIPS protected area is directly connected to the engine bleed port (EBP) in each nacelle. Each EBP supplies bleed air to one of the two pneumatic system manifolds (PS-L and PS-R) located in the aft body. Both ECS packs are directly connected to a manifold. When the aircraft is parked with main engines shut, ECS packs may be driven by APU bleed air which flows through a central cross-bleed duct between the manifolds. The WIPS protected area is supplied through a long duct routing from the manifolds via side of the fuselage, and a WIPS cross-bleed duct over the cabin is introduced for redundancy.

For More Electric architectures, certain pneumatic ducts and valves are eliminated, and the connectivity is determined using the following rules:

1. If the ECS is electrified, the APU supply duct and ECS pack supply ducts are removed.
2. If the WIPS is electrified, the ducts connecting pneumatic system manifolds and wing ice protection valves are removed; the WIPS cross-bleed duct and valve are also removed.
3. If the CIPS is electrified, the duct connecting engine bleed port and nacelle front face in each nacelle is removed.
4. If both ECS and WIPS are electrified, the ducts connecting engine bleed ports and pneumatic system manifolds are removed.

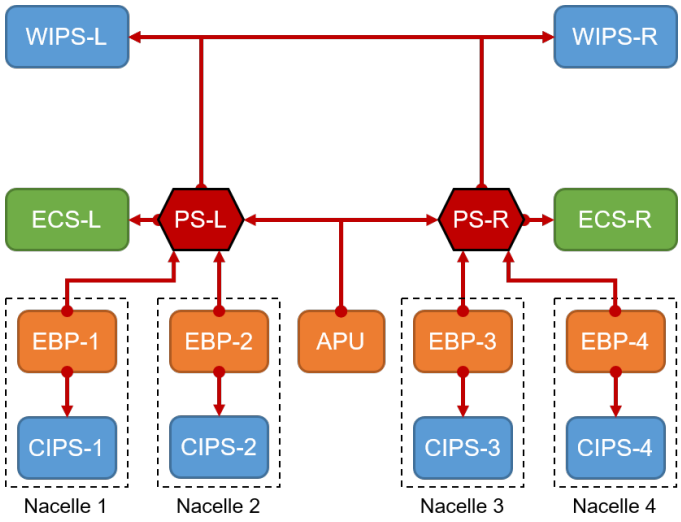


**Figure 7. Topological diagram of connection between pneumatic IPS, ECS and bleed sources**

In More Electric architectures, the remaining ducts, heat exchangers, and valves are downsized based on the required air mass flow rate. In All Electric architectures where no PCS consumes pneumatic power, the entire PPGDS is eliminated.

### B. Hydraulic Power Generation and Distribution System

The hydraulic power generation and distribution system (HPGDS) exists only if the selected actuation package uses actuators which consume hydraulic power as specified in Table 2. The mass of the hydraulic pipes (including the hydraulic fluid) is determined in the following way: first, the wall thickness is estimated based on circumferential stress; then the linear density (mass per unit length) of the pipe is computed as a function of the volumetric flow rate, flow velocity, wall thickness, and the density of pipe material and hydraulic fluid; finally, after mapping the topological diagram to the physical connectivity, the mass of each segment of hydraulic pipe can then be computed based on its length and linear density. In More Electric architectures, some hydraulic pipes are removed and the rest downsized. In All Electric architectures, the entire HPGDS is eliminated.

### C. Electric Power Generation and Distribution System

The electric power generation and distribution system (EPGDS) always exists due to invariant electrical loads such as avionics, radio, lighting, in-flight entertainment, and galley, which are always present regardless of the architecture selected. In this work, the connectivity within EPGDS mainly focuses on the subsystems which consume either pneumatic power or hydraulic power in some architectures but are electrified in More Electric architectures.

The layout of EPGDS is first defined parametrically in the topological diagram and then translated to physical connectivity based on the sized aircraft. The cables are sized based on the peak power requirements of the downstream power consumers. The mass of a conductor of length $L$ transmitting peak power $P_{\text{in}}$ is computed as[14]

$$M_{\text{cbl}}(P_{\text{in}}, L) = K_{\text{cbl-wt}} \kappa_{\text{inst}} \mathcal{K}_{\text{cbl}} P_{\text{in}} L \tag{5}$$

where $K_{\text{cbl-wt}}$ is a multiplicative factor modeling the uncertainty in the computed cable mass with a nominal value of 1 (to be addressed in Sec. VII-B); $\mathcal{K}_{\text{cbl}}$ is a characteristic parameter of the conductor depending on the circuit type (AC or DC) and operating voltage; the installation factor $\kappa_{\text{inst}}$ accounts for the mass for additional wirings length required to avoid obstacles. For a More Electric or All Electric architecture, the engine and APU generators may need upsizing to meet the increase in electric power requirements.

### D. Mechanical Power Generation and Distribution System

The mechanical power generation and distribution system (MPGDS) is responsible for converting engine shaft-power to hydraulic and electric power. By definition, the MPGDS control volume only contains the accessory gearbox. The mass and mechanical loss due to power transmission are computed following the methods described in Chakraborty's work.[13] Higher shaft-power requirement leads to heavier accessory gearbox.

### E. Secondary Power Extraction Penalties

The engine fuel flow at a certain thrust level is affected by both shaft-power and bleed extraction. This penalty depends on engine design parameters, flight condition, and thrust level, and typically shows a non-linear relation with respect to the secondary power extraction. While a physics-based parametric engine model may be used to evaluate the secondary power extraction penalties in NPSS, numerical issues occasionally cause failure of convergence at unpredictable engine operating conditions. In most cases, the issues can be resolved by manually rerunning the failed cases. However, these convergence issues and convergence time make it infeasible to make direct incorporation of such a NPSS engine model into ISSAAC for batch mode analyses. To enable fast evaluation and avoid the convergence issue in NPSS, a multi-level and multi-dimensional surrogate engine model is generated off-line prior to ISSAAC execution, by sampling the engine fuel flow ($\dot{W}_f$) at different operating conditions, which include flight altitude ($h$), freestream Mach number ($M_\infty$), thrust per engine ($T$), shaft-power extraction per engine ($P_{\text{spx}}$), and bleed extraction per engine ($\dot{m}_{\text{bx}}$). The surrogate model, which is queried by ISSAAC, has the form shown in Eq. (6):

$$\dot{W}_f = f(h, M_\infty, T, P_{\text{spx}}, \dot{m}_{\text{bx}}) \tag{6}$$

The time-varying fuel penalty per engine due to secondary power extraction ($\Delta\dot{W}_{f,\text{sp}}(t)$) can therefore be obtained by querying the surrogate model twice and taking the difference, as shown in Eq. (7):

$$\Delta\dot{W}_{f,\text{sp}}(t) = f(h(t), M_\infty(t), T(t), P_{\text{spx}}(t), \dot{m}_{\text{bx}}(t)) - f(h(t), M_\infty(t), T(t), 0, 0) \tag{7}$$

In this study, two engine models are considered: a mixed off-take engine model (E1), and another engine model (E2) which is sized for pure shaft-power requirements corresponding to 200% increase compared to E1. These physics-based engine models are created using multiple design approach used in Ozcan et al.'s work.[20] In ISSAAC V2, if an architecture consumes no bleed, i.e., WIPS $\geq 2$, CIPS $\geq 2$, and ECS $= 1$, then the E2 meta-model will be used to evaluate the shaft-power and drag penalty; otherwise, the E1 meta-model is queried.

## VI. Evaluation of Off-Design Mission Performance

Each commercial aircraft is sized for a certain design mission, i.e., a specified combination of design range and design payload weight, plus other performance and geometric constraints. However, in real-world operation, aircraft more often perform off-design missions, which, in terms of range and payload, may be shorter but heavier, longer but lighter, or even both shorter and lighter compared to their design mission. For some off-design missions where the aircraft takes off at nearly maximum takeoff weight (MTOW) or with nearly full fuel, an alternative subsystem architecture could potentially make such missions no longer feasible if there is adverse impact on aircraft operating empty weight (OEW), drag polar, and/or specific fuel consumption (SFC). Therefore, besides the design mission performance, it is also important to study the impact of subsystem architectures on off-design mission performance.

In ISSAAC V2, once the vehicle and subsystem architecture has been sized, off-design mission performance may be evaluated using FLOPS with appropriate $RERUN and corresponding $MISSIN and (if any) $PCONIN namelists.[16] Additional information required for off-design mission performance evaluation includes the maximum payload weight and maximum fuel capacity. Figure 8 presents a nominal payload-range diagram showing all four types of missions which can be evaluated in ISSAAC V2. There are five evaluation modes (Modes 1–5) which concern different types of off-design missions, summarized in Table 7. For completeness, this table also includes Mode 0 where only the design mission is evaluated. The three types of off-design missions are briefly described in the subsections.

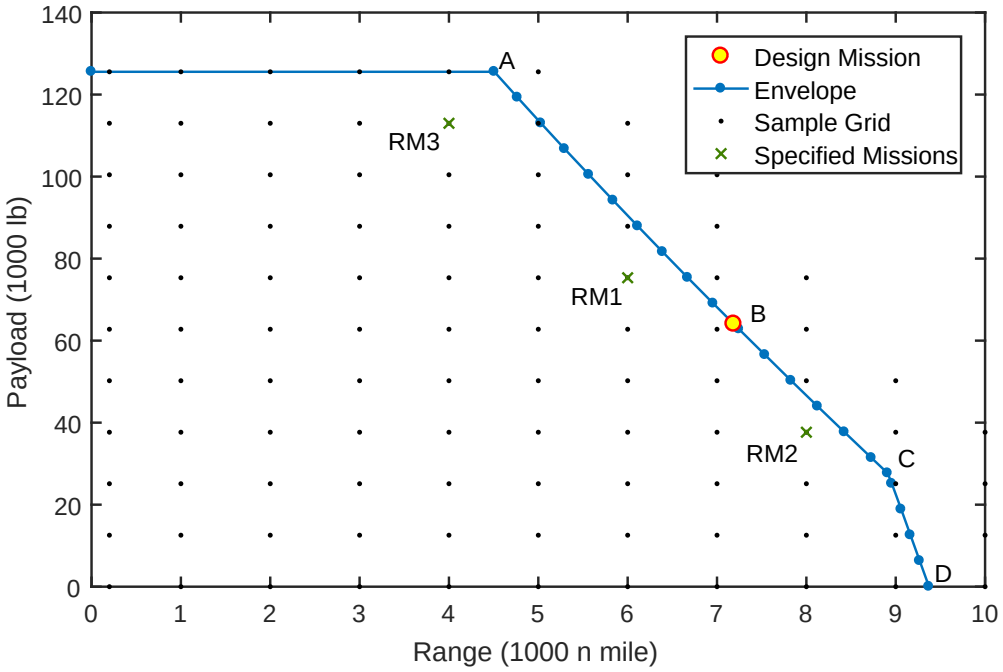


**Figure 8. Payload-range diagram showing all mission types evaluated by ISSAAC V2**

**Table 7. Mission analysis modes in ISSAAC V2**

| Mission Type | Mode 0 | Mode 1 | Mode 2 | Mode 3 | Mode 4 | Mode 5 |
|---|---|---|---|---|---|---|
| Design mission | ✓ | ✓ | ✓ | ✓ | ✓ | ✓ |
| Payload-range envelope | | ✓ | ✓ | ✓ | ✓ | |
| Sample grid | | | ✓ | | ✓ | |
| Specified off-design mission(s) | | | | ✓ | ✓ | ✓ |

### A. Payload-Range Envelope

Each point along the inclined sections of the payload-range envelope $(R_{\max}, W_p)$ indicates the maximum range of the vehicle carrying certain amount of payload. ISSAAC V2 generates a one-dimensional grid on payload weight, then computes the maximum range at each payload level by solving the following constrained maximization problem for a sized aircraft:

$$\begin{aligned} \max_{W_f} \quad & R = f(W_f, W_p) \\ \text{s.t.} \quad & W_R = W_e + W_p + W_f \\ & W_R \leq W_{R,\max} \\ & W_f \leq W_{f,\max} \end{aligned} \tag{8}$$

where $W_R$ is the gross weight at engine start, $W_e$ is the operating empty weight, $W_p$ is the payload weight, and $W_f$ is the mission fuel weight (weight of fuel onboard at engine start). The objective, the mission range $R$, is computed by FLOPS. To capture key points on the envelope, the following four cases labeled in Fig. 8 are always evaluated regardless of the user-specified resolution of payload weight:

- Point A: The aircraft carries maximum payload and certain amount of fuel such that it departs at $W_{R,\max}$. The corresponding range is called the harmonic range.

- Point B: The aircraft carries the design payload and as much fuel as possible such that no constraint is violated. For retrofit, the maximum range in this case is not necessarily equal to the design range.
- Point C: The aircraft carries maximum fuel and certain payload such that it departs at $W_{R,\max}$.
- Point D: The aircraft departs with maximum fuel and no payload, while the gross weight is less than $W_{R,\max}$. The corresponding range is called the ferry range.

The payload-range envelope encloses all feasible off-design missions and forms a feasible mission space. Switching between subsystem architectures may result in change in vehicle operating empty weight, aerodynamic characteristics, and propulsion system characteristics, which in turn influence the shape of the envelope. When assessing the impact of two subsystem architectures on mission-related metrics such as gross weight, mission fuel (required fuel on board prior to engine start, including reserve fuel), and block fuel (fuel burned between engine start and shutdown), etc., comparison is only valid in the intersection of the two feasible mission spaces, i.e. the mission space that is common to both designs being compared.



### B. Sample Grid

Once the payload-range envelope is determined, a two-dimensional grid on payload weight and mission range can be generated inside and near the envelope. Each grid point represents an off-design mission which is evaluated in ISSAAC V2. Results from evaluation of the grid may be used to generate surrogate models in the general form of

$$Q = f(R, W_p) \tag{9}$$

Examples of metric $Q$ include takeoff gross weight, mission fuel, block fuel, flight time, and average specific range (range per unit weight of block fuel), etc. The surrogate model $f$ is by default a linear interpolating model, which is sufficiently representative if the metric is expected to vary smoothly within the feasible mission space; more complex models such as polynomial response surface equations and radial basis functions may also be generated in post-processing using the original data from the sample grid, depending on variation of the metric. The surrogate models may be used to perform fast evaluation of any off-design mission inside the payload-range envelope, to generate contour plots, and to investigate the impact of a subsystem architecture on the entire feasible mission space.

### C. Specified Missions

A few off-design missions, each specified by range and payload weight, may be directly evaluated in ISSAAC V2 instead of using the surrogate model based on the interior grid, in order to eliminate model representation errors. These off-design missions are meant to represent payload-range combinations which are most commonly or typically flown by the aircraft. Data of the specified off-design missions may be used to conduct sensitivity analyses on epistemic uncertainties, technology state-of-the-art, and operational parameters for a given subsystem architecture.

In this work, three off-design missions inside the payload range envelope (labeled in Fig. 8) are selected as the reference missions (RM) to investigate the impact of subsystem architecture and uncertainty factors. As shown in Table 8, RM1 is closest to the baseline design mission (7310 n mile range, 64,050 lb payload), RM2 is a long-range mission with lighter paylaod, and RM3 is a short-range mission with heavier payload. The payload fraction indicates the ratio between the mission payload and the maximum permissible payload (125,550 lb).

**Table 8. Reference off-design missions**

| ID | Range (n mile) | Payload Weight (lb) | Payload Fraction |
|---|---|---|---|
| RM1 | 6000 | 75,330 | 60% |
| RM2 | 8000 | 37,665 | 30% |
| RM3 | 4000 | 112,995 | 90% |

# VII. Vehicle-level Performance and Sensitivity Assessment of Subsystem Architectures

This section describes the evaluation of HWB subsystem architectures mentioned in Table 3. The following metrics are considered:

- Aircraft operating empty weight (OEW): The impact on OEW is represented by the percentage change in OEW, normalized by the OEW of the baseline (Architecture 0000).
- Block fuel (BF): This includes the percentage change in BF for the three reference missions, normalized by the corresponding BF of the baseline. A decrease in BF of all reference missions is desirable.
- Range capability: This include the change in nominal range (maximum range at design payload), harmonic range, and ferry range relative to those of the baseline. Increases in these ranges are desirable.

Section VII-A presents the predicted weight, range capability, and fuel performance of all considered architectures. Section VII-B investigates the impact of various sources of uncertainty on a down-selected group of architectures.



## A. Evaluation of Subsystem Architecture Space

An assessment of the selected 224 architectures mentioned in Table 3 is first made by performing a full-factorial design of experiment (DoE) over the entire architecture space, from which a profiler plot is constructed to observe the impact of different architectures, as shown in Fig. 9. The two technology profilers are evaluated at Architecture 0000 (conventional baseline) and 6331 (an All Electric architecture), respectively. The $y$-coordinate of the crosshair indicates the impact on weight, range, and fuel burn of the architecture specified on $x$-axis. For each subsystem, the impact of switching its architecture from one to another (holding the architecture of all other subsystems) is represented by the difference in $y$-coordinates of the currently specified and target architectures. The $y$-axis intervals are identical within the group of ranges (row 2-4) and the group of BF (row 5-7), respectively, so that the impact of subsystem architectures may be visually compared across the rows within either group. Following are some observations made from Fig. 9:

- More Electric actuation functions (nonzero AFP numbers) show improvements in all metrics compared to AFP-#0. Although the electric actuators are generally heavier than the hydraulic ones when sized to provide the same power/force output, the weight reduction from replacing hydraulic lines with electric cables counteracts the weight increase in the actuators, thus reducing the overall fuel burn. However, the overall impact is marginal, and subject to uncertainties.
- For WIPS, switching from architecture 0 (pneumatic evaporative anti-icing) to 1 (pneumatic running-wet anti-icing) results in significant range extension, fuel saving, and OEW reduction, since the change in sizing condition reduces the sizing power, which leads to down-sizing of the pneumatic ducts and reduction in bleed extraction (hence fuel saving). Electrification of WIPS ($1 \rightarrow 2$) alone, while keeping all other subsystems conventional, results in minor decrease in range and increase in OEW, but the fuel performance is hardly affected. Finally, switching from electro-thermal anti-icing to de-icing WIPS ($2 \rightarrow 3$) gives further range extension, OEW decrease, and small amount of additional fuel saving.
- Compared to the pneumatic CIPS architectures (0 and 1), simply switching to electric architectures (2 and 3) without changing the engine design shows a degradation in OEW and the ranges, while the impact on fuel burn is marginal.
- The impact of ECS architecture on the key ranges shows opposite trends. When ECS is switched from pneumatic (0) to electric (1) architecture, significant addition of hardware mass reduces the available fuel quantity at takeoff when the gross weight is an active constraint. Therefore, since both the nominal range and the harmonic range are constrained by the maximum gross weight, they gain less benefit compared to the ferry range which is constrained by the fuel capacity. Also, the fuel saving with electric ECS is seen slightly higher for longer missions.
- The impact of engine architecture can be seen in the profiler plot evaluated at Arch. 6331. Compared to the profiler at Arch. 0000, the more significant improvements in ranges and fuel burn (indicated by

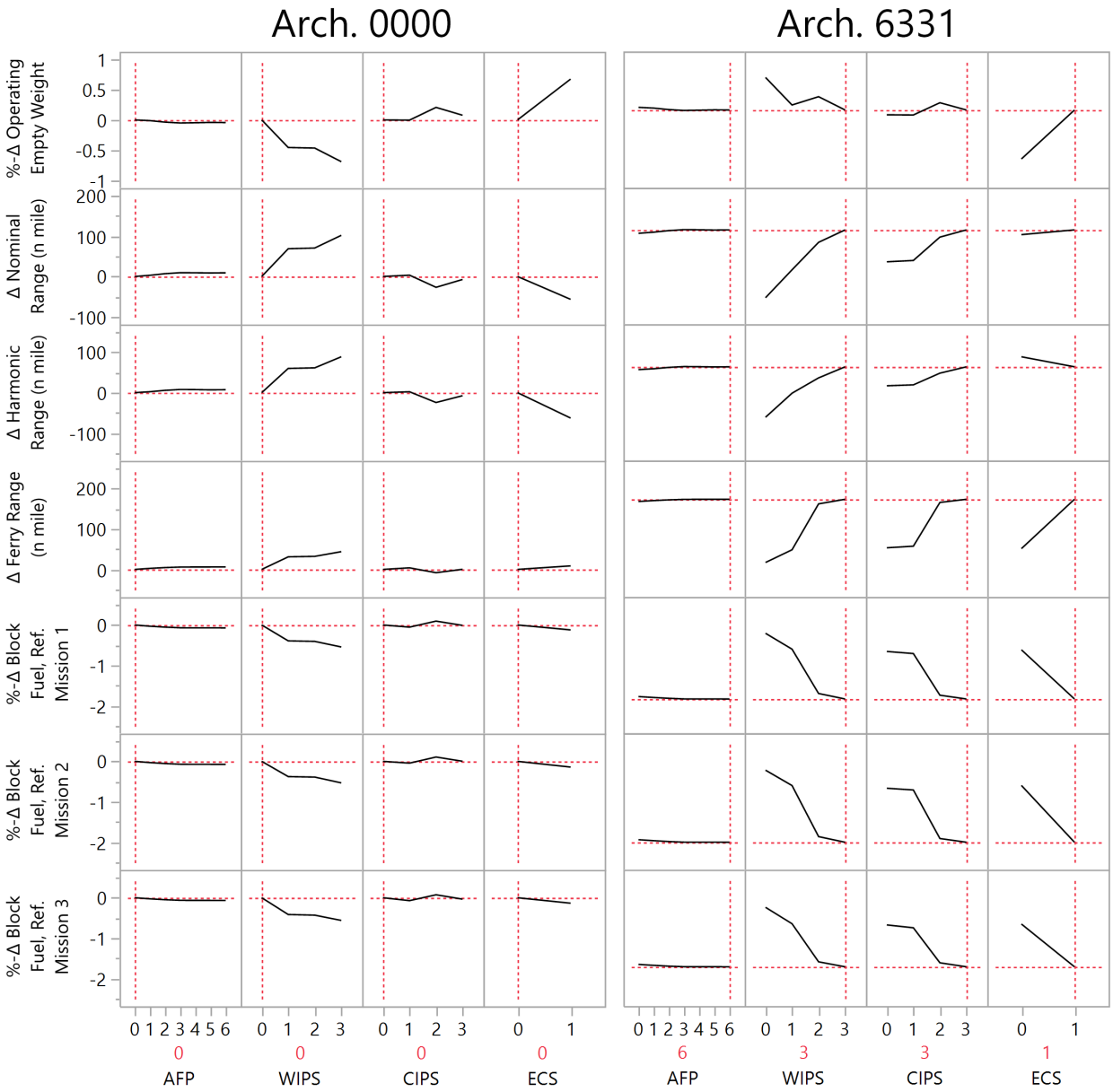


**Figure 9. Impact of individual subsystems**

the different slopes) between WIPS $= 1 \rightarrow 2$, CIPS $= 1 \rightarrow 2$, and ECS $= 0 \rightarrow 1$ result from switching between the conventional mixed off-take engine (E1) and the bleedless engine (E2). This implies that shaft-power is more efficiently extracted from E2 than from E1, yielding less fuel penalty for the same amount of shaft-power off-take.

Figure 10 presents the performance impact of the 224 considered subsystem architectures, where areas of degraded/deteriorated fuel burn, OEW, and range are indicated by shaded areas. Observations from this figure are as follows:

- Compared to the conventional baseline, all architectures with electric ECS show an increase in OEW and improvements in fuel burn. However, unless WIPS and CIPS architectures are already electric (2 or 3), electrification of ECS alone does not result in change of engine architecture, therefore it yields marginal improvement in fuel burn, while increasing the OEW and reduces the nominal range.
- The overall benefit of the bleedless architectures can be seen from the separate clusters of points

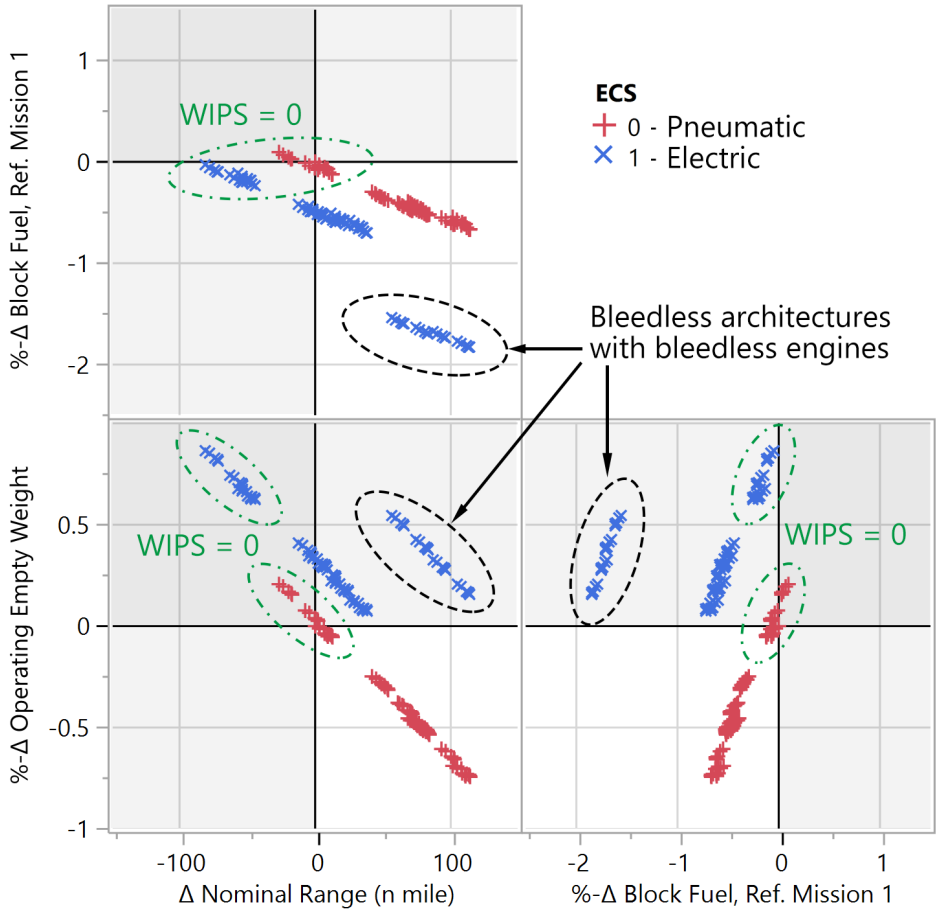


**Figure 10. Comparison of 224 subsystem architectures**

as indicated in Fig. 10, which exhibit significant fuel advantage over the candidates which still use pneumatic power and mixed off-take engines.

- For a given ECS architecture, candidates with WIPS $= 1, 2,$ and 3 show significant improvement in nominal range and fuel burn, meanwhile reducing the OEW, compared to those with WIPS $= 0$, as indicated in Fig. 10. The three beneficial architectures are sized for running-wet instead of evaporative requirements, which reduces the secondary power consumption and leads to down-sizing of WIPS components. Compared to a conventional large twin-aisle TW vehicle, the HWB300 baseline layout has longer pneumatic ducts connecting the WIPS to the pneumatic system manifolds (as seen in Fig. 6 and 7), down-sizing of the ducts and replacing them with electric cables has a major impact on all considered metrics.

## B. Sensitivity to Epistemic and Technological Uncertainties

A total of nine K-factors are selected to model the effect of epistemic uncertainty and variation of technological state-of-the-art (SOTA). The epistemic uncertainty arises from lack of knowledge in the early design phase, specifically due to assumptions and simplifications during the modeling process. Since it is difficult to accurately predict the technological SOTA at the estimated entry-into-service of the aircraft concept, especially for newer technologies on steep development curves, uncertainty in such prediction may become considerably high. This work considers the impact of five epistemic uncertainty factors and four SOTA uncertainty factors, whose definition is consistent with Chakraborty and Mavris' previous work.[15] A concise description of the K-factors follows:

- Epistemic uncertainty K-factors

- $K_{\text{act-loads}}$: multiplicative factor for the computed actuation loads or power requirements in all actuation functions (FCAS, TRAS, NWSS, WBS, and LGAS).
- $K_{\text{ecs-load}}$: multiplicative factor for the computed internal heat load seen by the ECS.
- $K_{\text{ips-load}}$: multiplicative factor for the computed heat rate requirement for WIPS and CIPS.
- $K_{\text{cable-wt}}$: multiplicative factor for the computed weight of electrical cables in EPGDS.
- $K_{\text{duct-wt}}$: multiplicative factor for the computed weight of pneumatic ducts in PPGDS.

- Technological SOTA K-factors
  - $K_{\text{em-sota}}$: multiplicative factor for the predicted power-to-mass ratio of electric motors, acting on all electrified actuation functions and electric ECS.
  - $K_{\text{pe-sota}}$: multiplicative factor for the predicted power-to-mass ratio of power electronics, acting on all electrified actuation functions, electric IPS and ECS, and EPGDS.
  - $K_{\text{cac-sota}}$: multiplicative factor for the predicted power-to-mass ratio of cabin air compressor (CAC), acting on electric ECS.
  - $K_{\text{gen-sota}}$: multiplicative factor for the predicted power-to-mass ratio of generators, acting on EPGDS.

Table 9 summarizes the K-factors and the subsystems affected by each of them. A central composite DoE is prepared using the MATLAB function `ccdesign` for each group of K-factors, where the nominal levels $\{-1, 0, +1\}$ in the DoE tables are mapped to the sampling levels of each K-factor in Table 9. The same DoEs are performed on a subset of four representative architectures: (1) Arch. 0000: a conventional architecture with hydraulic actuations, pneumatic WIPS, CIPS, and ECS; (2) Arch. 6000: a More Electric architecture with electrified actuations, pneumatic WIPS, CIPS, and ECS; (3) Arch. 0331: a bleedless architecture with hydraulic actuations, electric WIPS, CIPS, and ECS; and (4) Arch. 6331: an All Electric architecture with electrified actuations, WIPS, CIPS, and ECS.

**Table 9. Summary of K-factors for uncertainty analysis**

| K-Factor | Subsystem(s) Directly Affected | Sampling Levels |
|---|---|---|
| | *Epistemic uncertainty K-factors* | |
| $K_{\text{act-loads}}$ | Actuation | $\{0.9, 1.0, 1.1\}$ |
| $K_{\text{ecs-load}}$ | ECS | $\{0.9, 1.0, 1.1\}$ |
| $K_{\text{ips-load}}$ | WIPS, CIPS | $\{0.9, 1.0, 1.1\}$ |
| $K_{\text{cable-wt}}$ | EPGDS | $\{0.9, 1.0, 1.1\}$ |
| $K_{\text{duct-wt}}$ | PPGDS | $\{0.9, 1.0, 1.1\}$ |
| | *Technological SOTA K-factors* | |
| $K_{\text{em-sota}}$ | Actuation, ECS | $\{0.5, 1.5, 2.5\}$ |
| $K_{\text{pe-sota}}$ | Actuation, IPS, ECS, EPGDS | $\{0.5, 1.5, 2.5\}$ |
| $K_{\text{cac-sota}}$ | ECS | $\{0.5, 1.5, 2.5\}$ |
| $K_{\text{gen-sota}}$ | EPGDS | $\{0.5, 1.5, 2.5\}$ |

For each DoE, a prediction profiler of a second-order polynomial response surface model is generated using the statistical analysis tool JMP, as shown in Fig. 11 and 12. Similar to the technology profilers in Fig. 9, for each metric, the length of $y$-axis intervals are identical across different Architectures. Also, the length of $y$-axis intervals are identical for the key ranges and BF in each figure. For example, in Fig. 11, the $y$-axes of the three ranges for both architectures span $\pm 5$ n mile centered at their current values. The K-factors in Fig. 11 and 12 are all set to their nominal values (unity) on the $x$-axes, and the height of each triangular indicator indicates the relative influence of the corresponding K-factor, which is computed by the local derivative of each metric at the current K-factor settings. A larger triangle and a steeper slope of the profiler curve imply that the K-factor has a stronger influence on the corresponding metric compared to the other K-factors.

### 1. *Sensitivity to Epistemic Uncertainty*

Figure 11 shows the impact of the epistemic uncertainty K-factors for the baseline conventional architecture 0000 and All Electric architecture 6331. The following observations are made:

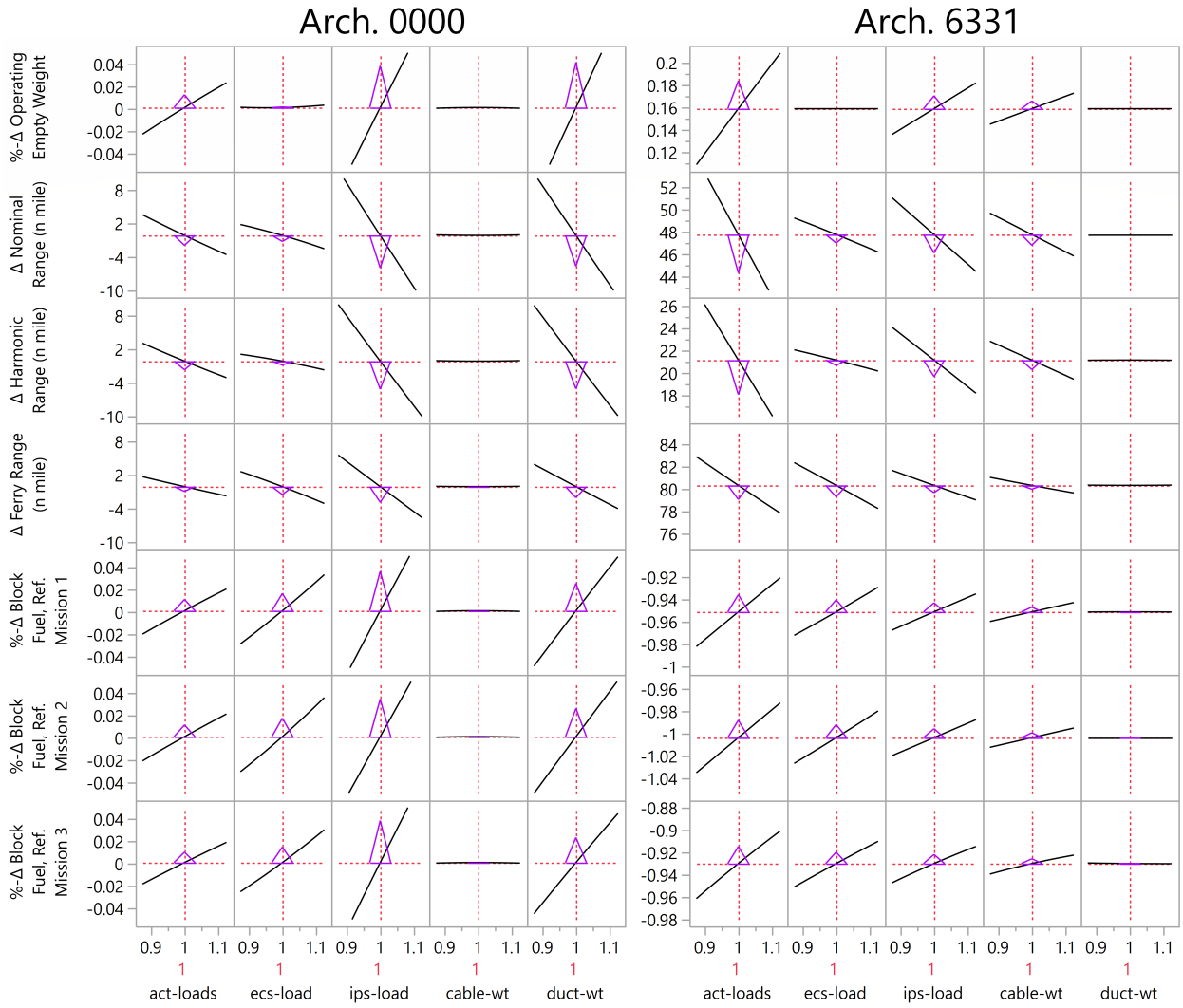


**Figure 11. Impact of epistemic uncertainty K-factors on vehicle-level metrics**

- For the same architecture, $K_{\text{act-loads}}$, $K_{\text{ips-load}}$, $K_{\text{duct-wt}}$ (Arch. 0000 only), and $K_{\text{cable-wt}}$ (Arch. 6331 only) have a greater impact on the nominal range and harmonic range than the ferry range. These K-factors have a direct impact on the sizing of actuators, pneumatic ducts, and electric cables, therefore have a stronger influences on the nominal range and harmonic range which are constrained by the maximum vehicle gross weight. The difference in the sensitivity of BF of the three reference missions to a certain K-factor is marginal, based on the similar slope in the same column in Fig. 11.

- $K_{\text{act-loads}}$ has a stronger impact on all metrics when the actuation functions are all electrified, since it is assumed that the electric actuator power-to-mass and force-to-mass ratios are lower than those of conventional hydraulic actuators with current SOTA. When the actuator sizing loads are varied at the same magnitude, the change in mass of the electric actuators are higher compared to hydraulic actuators, which in turn affects the OEW, and therefore the ranges and BF.

- $K_{\text{ecs-load}}$ has marginal impact on OEW for both architectures, since the range of thermal load variation does not require or requires a small increase in cabin supply air mass flow, which does not lead to

significant upsizing of ECS components. However, increasing ECS heat load requires an increase in cooling ram air mass flow, which in turn increases the ram drag, hence negatively affecting range and fuel burn.

- $K_{\text{ips-load}}$ has a stronger impact on conventional IPS than on electric IPS. The variation of required heat rate causes change in sizing power requirements for IPS, which in turn affects the mass of ducts (for pneumatic IPS) or cables (for electric IPS). Since IPS operates for a small time interval over the course of the mission, the fuel impact due to secondary power extraction is expected marginal, and therefore the change in OEW has a major contribution in the variation of ranges and BF.

- $K_{\text{cable-wt}}$ and $K_{\text{duct-wt}}$: These factors directly affect the estimated mass of electric cables and pneumatic ducts, respectively. For Arch. 0000 where ECS and IPS both consume pneumatic power, $K_{\text{duct-wt}}$ has a more significant impact than $K_{\text{cable-wt}}$, whereas for Arch. 6331 where the pneumatic system is completely eliminated, $K_{\text{duct-wt}}$ has no influence on the vehicle, while the impact of $K_{\text{cable-wt}}$ is seen higher due to electrification of the PCS.

### 2. *Sensitivity to Technological State-of-the-Art*

Figure 12 shows the impact of the technology SOTA uncertainty K-factors for unconventional architecture 6000, 0331, and 6331. The following observations are made:

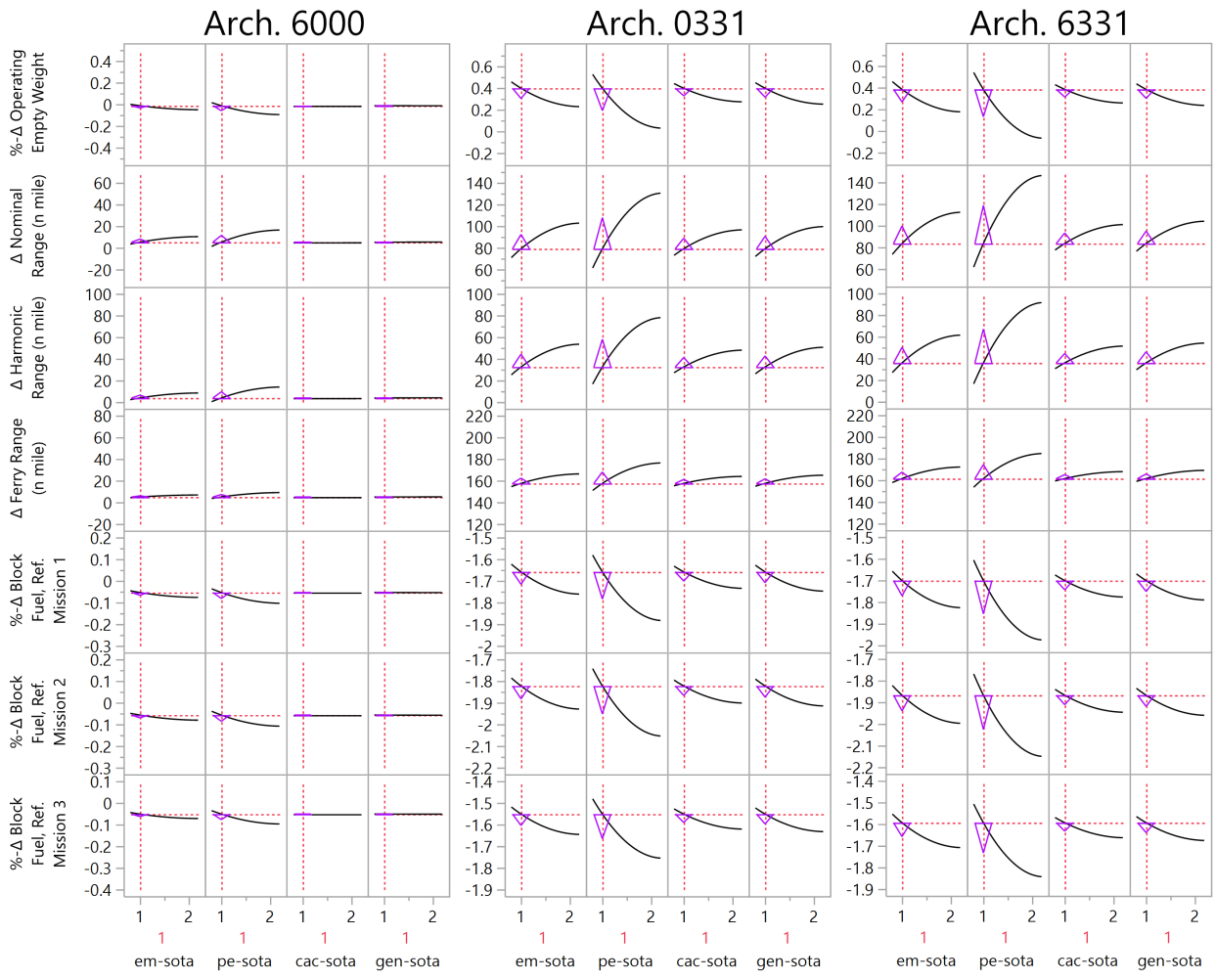


**Figure 12. Impact of SOTA uncertainty K-factors on vehicle-level metrics**

- In general, since these K-factors only affect the mass of subsystems that are electrified, an architecture involving more electrified actuation functions and subsystems has higher sensitivity to the considered SOTA K-factors. It can be seen that the All Electric Arch. 6331 shows the highest sensitivity to these K-factors.
- $K_{\text{em-sota}}$ has the greatest impact on Arch. 6331, since the electric motors are present in all electric actuators and the CACs.
- $K_{\text{pe-sota}}$ has the greatest impact on all metrics among the four SOTA K-factors considered. Since the power rating of the power electronics are assumed proportional to the rating of their downstream motors and power consumers, the impact of this K-factor is much more significant for Arch. 0331 and 6331 where the CACs consume a large amount of electric power.
- $K_{\text{cac-sota}}$ has no impact on the pneumatic ECS. For electric ECS, this K-factor directly affects the mass of the CACs, but its impact is less than $K_{\text{pe-sota}}$.
- $K_{\text{gen-sota}}$ has a more significant requirement when the capacity of the on-board generators need to be increased. This happens for Arch. 0331 and 6331 where the presence of electric IPS and ECS requires more electric power than the baseline generators can provide.

## VIII. Conclusions

This work considers the sizing and analysis of various subsystem architectures in the early design phase of a novel HWB vehicle. The vehicle-level performance of different subsystem architectures are evaluated using an enhanced version of Integrated Subsystems Sizing and Architecture Assessment Capability. In a retrofit scenario, the impact of subsystem architectures and uncertainty factors is assessed by investigating the change in vehicle operating empty weight, key range capabilities, and mission fuel burn relative to a baseline 300-pax class HWB vehicle with a conventional subsystem architecture. Physics-based modeling and sizing methods are adopted for most subsystem components with the lack of historical data. Surrogate models of ECS packs and turbofan engines constructed from high-fidelity physical models are incorporated in ISSAAC V2 to enable fast evaluation of subsystems sizing and mission performance analysis and automatic evaluation of a large architecture space. Off-design mission performance is assessed since the same type of commercial aircraft can operate a wide range of missions in real world. An evaluation of the entire architecture space with 224 architectures reveals that bleedless architectures show significant improvements in range and fuel saving because shaft-power is extracted with less fuel penalty from a bleedless engine than from a conventional mixed off-take engine. The power requirement of WIPS also has a strong impact on OEW, range, and fuel burn. Sensitivity analyses are performed to investigate the impact of uncertainty factors, which shows that the uncertainty in IPS heat rate has the strongest impact on conventional architecture, while the All Electric architecture is more sensitive to the actuation loads. It is also observed that substantially electrified architectures are more sensitive to uncertainty in technological SOTA. Possibilities for future work include: (1) an integrated sizing capability of the HWB vehicle, engine, and subsystems; (2) modeling of novel subsystems on HWB such as the hybrid-electric propulsion systems, flow control system, etc.; and (3) evaluation of subsystem architectures for HWB vehicles of different sizes.

## References


[1]Mangelsdorf, M., "Environmentally Responsible Aviation N+2 Advanced Vehicle Concepts NRA Status," June 2011.

[2]Liebeck, R. H., "Design of the Blended Wing Body Subsonic Transport," *Journal of Aircraft*, Vol. 41, No. 1, Jan. 2004, pp. 10–25.

[3]Nickol, C. and Mccullers, L., "Hybrid Wing Body Configuration System Studies," *47th AIAA Aerospace Sciences Meeting including The New Horizons Forum and Aerospace Exposition*, American Institute of Aeronautics and Astronautics (AIAA), Jan. 2009.

[4]Felder, J. L., Brown, G. V., DaeKim, H., and Chu, J., "Turboelectric distributed propulsion in a hybrid wing body aircraft," 2011.

[5]Nickol, C., "Hybrid Wing Body Configuration Scaling Study," *50th AIAA Aerospace Sciences Meeting including the New Horizons Forum and Aerospace Exposition*, American Institute of Aeronautics and Astronautics (AIAA), Jan. 2012.

[6]Garmendia, D. C., Chakraborty, I., and Mavris, D. N., "Method for Evaluating Electrically Actuated Hybrid Wing–Body Control Surface Layouts," *Journal of Aircraft*, Vol. 52, No. 6, Nov. 2015, pp. 1780–1790.

[7]Garmendia, D. C., Chakraborty, I., and Mavris, D. N., "Multidisciplinary Approach to Assessing Actuation Power of a Hybrid Wing–Body," *Journal of Aircraft*, Vol. 53, No. 4, July 2016, pp. 900–913.

[8]Gern, F. H., "Conceptual Design and Structural Analysis of an Open Rotor Hybrid Wing Body Aircraft," *54th AIAA/ASME/ASCE/AHS/ASC Structures, Structural Dynamics, and Materials Conference*, American Institute of Aeronautics and Astronautics (AIAA), April 2013.

[9]Laughlin, T., Corman, J., and Mavris, D., "A Parametric and Physics-Based Approach to Structural Weight Estimation of the Hybrid Wing Body Aircraft," *51st AIAA Aerospace Sciences Meeting including the New Horizons Forum and Aerospace Exposition*, American Institute of Aeronautics and Astronautics (AIAA), Jan. 2013.

[10]Cloyd, J., "Status of the United States Air Force's More Electric Aircraft initiative," *IEEE Aerospace and Electronic Systems Magazine*, Vol. 13, No. 4, April 1998, pp. 17–22.

[11]Sinnett, M., "Boeing 787 No-Bleed Systems: Saving Fuel and Enhancing Operational Efficiencies," Boeing Aero Magazine, Quarter 4, 2007, Online: http://www.boeing.com/commercial/aeromagazine/, 2007.

[12]Thomas, R., Burley, C., and Olson, E., "Hybrid Wing Body Aircraft System Noise Assessment with Propulsion Airframe Aeroacoustic Experiment," *16th AIAA/CEAS Aeroacoustics Conference*, American Institute of Aeronautics and Astronautics (AIAA), June 2010.

[13]Chakraborty, I., *Subsystem architecture sizing and analysis for aircraft conceptual design*, Ph.D. thesis, Georgia Institute of Technology, 2015.

[14]Chakraborty, I. and Mavris, D. N., "Integrated Assessment of Aircraft and Novel Subsystem Architectures in Early Design," *Journal of Aircraft*, Dec. 2016, pp. 1–15.

[15]Chakraborty, I. and Mavris, D. N., "Assessing Impact of Epistemic and Technological Uncertainty on Aircraft Subsystem Architectures," *Journal of Aircraft*, Dec. 2016, pp. 1–19.

[16]McCullers, L., *Flight Optimization System, Release 8.11, User's Guide*, NASA Langley Research Center, Hampton, VA 23681-0001, Oct. 2009.

[17]Lytle, J. K., "The Numerical Propulsion System Simulation: An Overview," NASA/TM—2000-209915, https://ntrs.nasa.gov/archive/nasa/casi.ntrs.nasa.gov/20000063377.pdf, June 2000.

[18]"Federal Aviation Regulations (FAR) Part 25 - Airworthiness Standards: Transport Category Airplanes," Federal Aviation Administration (FAA), U.S. Department of Transportation, online: http://www.ecfr.gov/.

[19]Shi, M., Chakraborty, I., Cai, Y., Tai, J. C., and Mavris, D. N., "Mission-Level Study of Integrated Gas Turbine and Environmental Control System Architectures," *AIAA SciTech Conference*, American Institute of Aeronautics and Astronautics (AIAA), Jan. 2018.

[20]Ozcan, M. F., Chakraborty, I., and Mavris, D. N., "Impact of Subsystem Secondary Power Requirements on Gas Turbine Sizing and Performance," *16th AIAA Aviation Technology, Integration, and Operations Conference*, 2016, p. 3146.